



Understanding the variability of the rainfall dipole in West Africa using the EC-Earth last millennium simulation

Qiong Zhang^{1,2} · Ellen Berntell^{1,2} · Qiang Li^{1,2} · Fredrik Charpentier Ljungqvist^{2,3,4}

Received: 31 May 2020 / Accepted: 8 February 2021 / Published online: 23 February 2021
© The Author(s) 2021

Abstract

There is a well-known mode of rainfall variability associating opposite hydrological conditions over the Sahel region and the Gulf of Guinea, forming a dipole pattern. Previous meteorological observations show that the dipole pattern varies at interannual timescales. Using an EC-Earth climate model simulation for last millennium (850–1850 CE), we investigate the rainfall variability in West Africa over longer timescales. The 1000-year-long simulation data show that this rainfall dipole presents at decadal to multidecadal and centennial variability and long-term trend. Using the singular value decomposition (SVD) analysis, we identified that the rainfall dipole present in the first SVD mode with 60% explained variance and associated with the variabilities in tropical Atlantic sea surface temperature (SST). The second SVD mode shows a monopole rainfall variability pattern centred over the Sahel, associated with the extra-tropical Atlantic SST variability. We conclude that the rainfall dipole-like pattern is a natural variability mode originated from the local ocean–atmosphere–land coupling in the tropical Atlantic basin. The warm SST anomalies in the equatorial Atlantic Ocean favour an anomalous low pressure at the tropics. This low pressure weakens the meridional pressure gradient between the Saharan Heat Low and the tropical Atlantic. It leads to anomalous northeasterly, reduces the southwesterly moisture flux into the Sahel and confines the Gulf of Guinea’s moisture convergence. The influence from extra-tropical climate variability, such as Atlantic multidecadal oscillation, tends to modify the rainfall dipole pattern to a monopole pattern from the Gulf of Guinea to Sahara through influencing the Sahara heat low. External forcing—such as orbital forcing, solar radiation, volcanic and land-use—can amplify/dampen the dipole mode through thermal forcing and atmosphere dynamical feedback.

Keywords West Africa rainfall dipole · Decadal to multidecadal variability · EC-Earth · Last millennium · Tropical Atlantic variability · Atlantic multidecadal oscillation

1 Introduction

West African rainfall is driven mainly by the West African monsoon (WAM) (Losada et al. 2010; Nicholson 2013; Sultan and Janicot 2003). Rainfall variability across various timescales is of great importance to ecosystems and

human life in West Africa. Most of the region’s population is largely dependent on rain-fed agriculture and pastures for livestock, making them highly vulnerable to rainfall fluctuations. Instrumental observation data over the past ~ 100 years indicate that western Africa rainfall shows significant variability on interannual, decadal, and multidecadal timescales (Mohino et al. 2011). For example, the semi-arid Sahel region experienced an intense and persistent drought during the 1970s and 1980s, which is one of the main recent climate variability signals (Caminade and Terray 2010; Dai et al. 2004; Folland et al. 1986; Giannini et al. 2003; Mohino et al. 2011; Rodríguez-Fonseca et al. 2011). The persistent Sahelian drought is widely covered worldwide by media for its dramatic socio-economic consequences, particularly food security (Kandji et al. 2006).

The interannual variability of the WAM is believed to be strongly related to nearby sea surface temperature (SST)

✉ Qiong Zhang
qiong.zhang@natgeo.su.se

¹ Department of Physical Geography, Stockholm University, Stockholm, Sweden

² Bolin Centre for Climate Research, Stockholm University, Stockholm, Sweden

³ Department of History, Stockholm University, Stockholm, Sweden

⁴ Swedish Collegium for Advanced Study, Uppsala, Sweden

anomalies, i.e. the SST anomalies over tropical and north Atlantic (Caminade and Terray 2010; Folland et al. 1986; Losada et al. 2010; Palmer 1986; Rodríguez-Fonseca et al. 2015; Zhang and Delworth 2006) or South Atlantic Ocean (Nnamchi and Li 2011). Observational data show that the SST anomalies in the tropical Atlantic are associated with a dipole rainfall patterns centred over the Sahel and the Gulf of Guinea (Janicot et al. 1998; Losada et al. 2010, 2012; Rodwell and Hoskins 1996; Ward 1998) before the 1970s. The dipole rainfall pattern disappeared after the 1970s, and change to a monopole rainfall pattern north of the Gulf of Guinea coast until 2000s (Janicot and Sultan 2001; Joly and Voldoire 2010). Losada et al. (2012) demonstrate with atmospheric modelling that the SST anomalies in tropical Atlantic alone can produce a rainfall dipole in West Africa. When the SST anomalies in the Atlantic appear accompanied by anomalies in the Indo-Pacific, the dipole pattern is drastically weakened. Studies have also shown a connection between Sahel rainfall and SST over the tropical Indian and Pacific Oceans (Palmer 1986; Xue et al. 2016). It is found that the Atlantic and Pacific SST have a comparable effect in reducing rainfall in the western Sahel. In contrast, the Indian Ocean SST reduces the rainfall in eastern Sahel (Palmer 1986). The impact from Pacific SST might be an indirect effect of the remote forcing on tropical Atlantic SST to influence the western African rainfall (Liu et al. 2004).

Previous studies have shown that multidecadal drought in West Africa during the instrumental period (past 100 years for Africa) is primarily driven by changing Atlantic SST patterns (Hoerling et al. 2006; Knight et al. 2006; Martin et al. 2014; Mohino et al. 2011; Ting et al. 2011a; Zhang and Delworth 2006). It suggests that these patterns may reflect a natural low-frequency mode from ~65 to ~80 years of SST variability: the Atlantic multidecadal oscillation (AMO) (Folland et al. 1986). Several studies also propose the possible impact of the Pacific decadal oscillation (PDO) on Western Africa rainfall (Mohino et al. 2011; Villamayor and Mohino 2015). However, climate models cannot skillfully capture the observed decadal to multidecadal WAM rainfall variability (Berntell et al. 2018; Martin et al. 2014; Masih et al. 2014; Mohino et al. 2011; Nouaceur and Murărescu 2016). Most global climate models underestimate the magnitude of decadal variability in the twentieth-century simulations (Biasutti 2013; Roehrig et al. 2013). The underestimation of hydroclimate variability at decadal and longer timescales is not a feature unique to the WAM but is common in other parts of the world (Ljungqvist et al. 2019a, b). This weak model-simulated decadal rainfall variability is not well understood but has so far received comparatively little attention. One reason for the models' shortcomings in simulating decadal-scale rainfall variability is likely related to coupled climate models' inability to realistically simulate the internally decadal SST variability—a key driver to

rainfall variability (Martin et al. 2014). The decadal climate variability in WAM has so far been tested in atmosphere-only models, with prescribed SST, and the problem remains unsolved (Berntell et al. 2018), pointing to unrealistically weak coupling between SST change and western African rainfall in model simulations.

The climate prediction and projection on decadal or longer timescales of western Africa rainfall are of central importance for the management of climate risk and vulnerability (Otero et al. 2016), therefore it is crucial that global climate models are capable of representing local as well as remote drivers of rainfall variability and the interaction between the two. This study has performed a 'last millennium' experiment from 850 to 1850 CE with an ocean–atmosphere coupled high-resolution global climate model EC-Earth (further details in Sect. 3.1 below). The results from 1001 years model output, from different diagnostic aspects such as the long-term trend, the centennial-scale climate change between Medieval Common Anomaly (MCA) and Little Ice Age (LIA), and rainfall variability at decadal to multidecadal timescales, all exhibit a dipole variability mode between the Sahel region and the Gulf of Guinea. We have investigated the possible drivers and dynamical processes in the coupled climate model system and found that this rainfall dipole pattern results from tropical-extratropical interaction in the north Atlantic basin. The external forcing can further amplify/dampen the dipole mode.

2 Dry and wet episodes from paleoclimate proxy data during the last millennium

The evaluation of the climate models' ability to capture the long-term climate variability largely depends on the study area's observational data. However, there are no continuous instrumental observation datasets available beyond the last ~100 years in West Africa. Moreover, relatively little paleoclimate proxy data is available for West Africa, and most have comparably low temporal resolution and relatively poor dating control (Nash et al. 2016). The region is located in the tropical to subtropical climate zones, with no glaciers to provide ice-core records. No long tree-ring records have successfully been produced, both due to the logistic challenges and because tropical trees do not grow reliable annual growth rings. Records from lake sediments are scarce because the shallow ponds and marshes dotting the region have dried during recent and past drought episodes (Nash et al. 2016). The most crucial proxy records come from Lake Chad in the Sahel region (Maley 1993) and Lake Bosumtwi at the Coast of Guinea (Shanahan et al. 2009; Talbot and Delibrias 1977) (highlighted in Fig. 1b). Sediments and pollen data from Lake Chad indicate comparatively wet

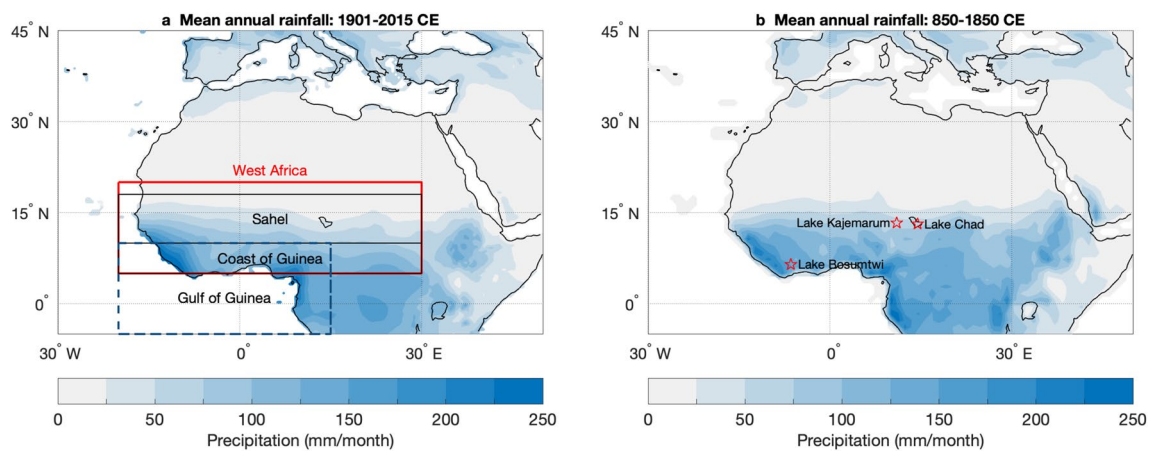


Fig. 1 Annual mean terrestrial rainfall (unit: mm/month) averaged from **a** CRU monthly data from 1901 to 2015, and **b** EC-Earth “last millennium” simulation from 850 to 1850. The red rectangle in **a** is the West Africa domain (5°–20° N, 20° W–30° E) defined in this study, the two sub-domains Sahel (10°–18° N, 20° W–30° E) and Coast of Guinea (5°–10° N, 20° W–30° E) are indicated with black

rectangles. The rainfall indices for these three regions are averaged respectively within the defined domain. The Gulf of Guinea, including the coastal area along the Gulf, is indicated with a dashed rectangle (5° S–10° N, 20° W–15° E). Three lakes in West Africa that provide the hydrological information during the last millennium are noted in **b**

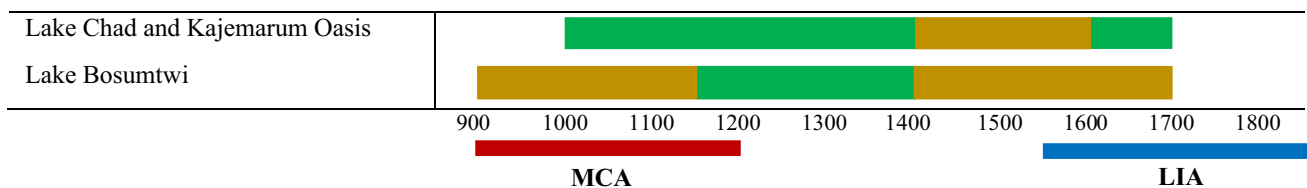
conditions prevailing ~ 1100–1400 CE and during the seventeenth century, whereas drier conditions prevailed during the fifteenth and sixteenth centuries (Maley 1993). Slightly wetter conditions in northeastern Nigeria during 1000–1200 CE are also apparent in sediment data from the dry lake floor of the Kajemarum Oasis (Street-Perrott et al. 2000), which is located about 400 km northwest of Lake Chad (see Fig. 1b). In the West African tropical region, the Lake Bosumtwi record shows drier conditions from 900 to 1150 CE (Shanahan et al. 2009), corresponding to more dust emissions recorded in marine sediment from offshore Senegal (Mulitza et al. 2010). After this dry episode, overlapping with the peak of the MCA globally, the region returned to wetter conditions until the early fifteenth century. These wetter conditions were followed by a persistent 300-year dry period from ~ 1450 to ~ 1750 CE, roughly overlapping with the significant portion of the LIA.

In Table 1, we summarised these wet-dry episodes during 850–1850 CE millennium. The changes in lake level recorded in Lake Bosumtwi indicated that West Africa

was even drier during the eighteenth century than during the twentieth century, implying the drought prevailing in the Sahel since the end of the 1960s is not exceptionally anomalous in the context of the past millennium (Shanahan et al. 2009).

These few available proxy records provide valuable information about the regional rainfall variability over longer timescales. The evidence from Lake Chad, Kajemarum Oasis and Lake Bosumtwi suggest that the out of phase hydrological conditions between subtropical and tropical West Africa occurs both during the MCA and the LIA. Although in phase hydrological conditions are also present, this indicates that the dipole variability observed in present-day rainfall even existed during 850–1850 CE and varies at centennial timescales (Table 1). These changes at centennial timescales are assumed to be associated with large-scale phenomena such as SST changes in the global oceans. How do these drivers modulate the rainfall variability over the region can be better-understood with ocean–atmosphere coupled climate model simulation.

Table 1 Dry (brown) and wet (green) episodes shown in sediments from the Lake Chad (Maley 1993), the Kajemarum Oasis (Street-Perrott et al. 2000), and the Lake Bosumtwi (Shanahan et al. 2009) during the last millennium



3 Climate model simulation and analysis methods

The period 850–1850 CE provides a comparatively well-documented history of multidecadal to multi-centennial climate changes, dominated by the MCA and LIA (Stocker et al. 2013). Thus ‘last millennium’ simulations are considered one of the key experiments in the Paleoclimate Modelling Intercomparison Project (PMIP) (Kageyama et al. 2018). We have run this simulation following the PMIP3 protocol. Several conventional statistical methods are applied to analyse the monthly mean model output. The statistically significant features from the analyses are presented and discussed.

3.1 The EC-Earth model and the experiment setup

We use the ocean–atmosphere coupled climate model EC-Earth (version 3.1) to perform the “last millennium” simulation. The EC-Earth model results from a consortium development effort from a group of different European research institutions (Hazeleger et al. 2012). EC-Earth’s atmospheric component is revised from the Integrated Forecasting System (IFS), which is developed at the European Centre for Medium-Range Weather Forecasts (ECMWF), coupled with a land model H-TESSSEL. The IFS and H-TESSSEL components are used to produce several ECMWF reanalyses widely used in climate research, e.g., ERA40, ERA-Interim, ERA20C and the latest ERA5. The ocean component is based on Nucleus for European Modelling of the Ocean (NEMO) (Madec 2008) including a sea-ice model LIM3 (Bouillon et al. 2009). The EC-Earth model has a relatively high resolution comparing the other climate models in PMIP3. The atmosphere’s horizontal resolution is 125 km, and 62 vertical layers; the ocean model NEMO has a horizontal resolution of 110 km with 40 vertical layers.

The climate forcing for the ‘last millennium’ experiment follows the PMIP3 protocol (Schmidt et al. 2011, 2012), with the orbital forcing calculated internally in the model following Berger (1978). Variations in total solar irradiance is based on the reconstruction provided by Vieira and Solanki (2010) for 850–1609 CE, and from 1610 CE on the reconstruction from Wang et al. (2005), and the volcanic aerosol forcing is from Crowley and Unterman (2013). Changes in greenhouse gas forcing are derived from Hansen and Sato (2004) and Macfarling Meure et al. (2006). Land-use changes are taken from Pongratz et al. (2008). All these imposed forcings vary from 850 to 1850 CE, and therefore this ‘last millennium’ simulation provides a 1001-year climate transient, containing both internal and externally forced

variability. The initial condition starts from an equilibrium state at 850 CE after a 300-year spin-up.

Our EC-Earth “last millennium” simulation has been completed after PMIP3; hence the model data are not presented in most of the PMIP3 “last millennium” model studies. We have included this dataset in a recent simulation-reconstruction comparison study evaluating the centennial-scale temperature changes together with other PMIP3 simulations (Ljungqvist et al. 2019b). The results of that study show that the EC-Earth is among the models that agree well with continental-scale temperature reconstructions for MCA and LIA changes. The EC-Earth “last millennium” simulation has also been used to estimate the maximum annual number of Atlantic tropical cyclones. The simulation has proved useful to statistically assess extreme climate events (Lavender et al. 2018).

Besides the ‘last millennium’ simulation, we performed a short ‘historical’ simulation from 1979 to 2009 using the CMIP5 historical forcing (Taylor et al. 2012). This ‘historical’ simulation is used to evaluate WAM rainfall’s climatology by comparing it to present-day instrumental observation data.

We use monthly mean rainfall, SST, sea level pressure, specific humidity, and horizontal wind at 850 hPa from the model output in the analysis. The simulated total rainfall is the sum of large-scale rainfall and convective rainfall. The moisture flux is calculated by humidity and horizontal wind field.

3.2 Instrumental observation data

Observational monthly mean rainfall and surface air temperature data derived from CRU TS 3.24.01 from Climate Research (Harris et al. 2014) are used to evaluate the model performance. The CRU dataset used land-based in-situ observations from meteorological stations across the globe and interpolated into a grid with 0.5° latitude by longitude resolution. The data length is 115 years covering 1901–2015. The availability of meteorological stations over Africa varies with time, i.e., 60–80% of the grid cells in Africa have station data for most of the twentieth century, with lower numbers at the beginning of the century and at the end. Grid cells lacking data are supplied with values equal to the 1961–1990 climatological mean.

The climatological annual mean rainfall shows an apparent difference from the northern arid Sahara to Guinea’s tropical coast, ranging from approximately 10 mm/month to 100 mm/month. We define our study region of West Africa as the domain 5°–20° N, 20° W–30° E. In regular model grids, it includes part of the adjacent Atlantic Ocean. The rainfall over the land area of this domain is averaged as a West Africa rainfall index. During the boreal summer months, the onset of the WAM shifts the monsoon rainfall northward. It leads to

more rainfall in the Sahel region, while the coastal area to the south, which we refer to as the Coast of Guinea, experiences a slightly decreased rainfall. Previous observation from station data shows that the year-to-year variability exhibits a strong contrast between the Sahel region and the Coast of Guinea (Janicot 1992; Janowiak 1988; Nicholson 1980; Nicholson and Palao 1993). The sign change in rainfall anomaly occurs approximately at 10° N (Janicot 1992). We further define two sub-region domain Sahel (10°–18° N, 20° W–30° E) and Coast of Guinea (5°–10° N, 20° W–30° E) to investigate the land area-averaged rainfall variability. In this study, the Gulf of Guinea refers to the equatorial Atlantic area at 5° S–5° N, 20° W–15° E, including a small part of the land area.

3.3 Statistical analysis method

To investigate the variability at different frequencies besides the long-term trend, we applied linear detrending using a least-square fit and filtering using a Butterworth filter (Emery and Thomson 2001). Two climate regimes, the MCA (900–1200 CE) and LIA (1550–1850 CE) are selected to address the centennial-scale climate change. The significance of the climate change between these two climate periods is examined using the two-sample *t*-test (Wilks 2011).

The relationship between the SST and West African rainfall is analysed using the singular value decomposition (SVD) analysis of the SST-rainfall cross-covariance matrix (Bretherton et al. 1992). The SVD analysis generalises empirical orthogonal function (EOF) analysis applied to two data fields (SST and rainfall in this case) together to identify modes that explain the largest covariance between the two fields. The expansion coefficients are time-series, one for each field, describing how the modes of variability oscillate in time. We calculate the homogeneous correlation between the expansion coefficients and their respective original field to visualise the covariance. To understand the mechanisms behind the covariance between SST and rainfall, regression maps are produced for sea level pressure (SLP), wind, humidity and moisture flux at 850 hPa against the two leading SVD expansion coefficients.

Power spectrum analysis is applied to calculate the periods on which the covariance varies. Here we use the multi-taper method (MTM) (Mann and Lees 1996), performed with the program *k*-spectra and parameters $p=3$, $K=5$. The peak periods' significance is calculated with the null-hypothesis that the peaks in the power spectrum are significantly larger than the red-noise spectrum at that frequency (Wilks 2011).

4 Results

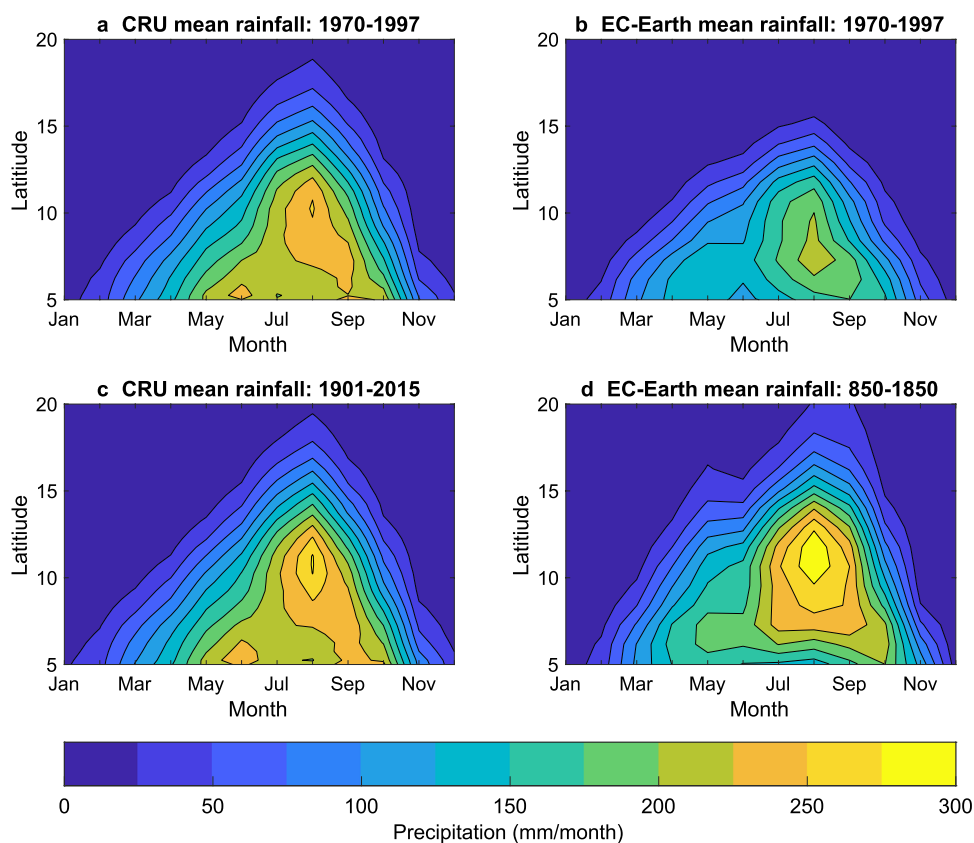
4.1 Model evaluation with instrumental observations

West Africa lies just south of the Sahara Desert (Fig. 1) and receives 768 mm annual mean rainfall (Fig. 1), decreasing from the south to north. There are two regional rainfall maxima in the West Africa domain. One is centred on the west coast around 5°–11° N, near the Cameroon highlands in eastern Coast of Guinea. There is a weaker rainfall maximum in the east part of the continent, over the Ethiopian highlands. The climatology from the EC-Earth last millennium simulation shows a very similar pattern.

The CRU rainfall data from 1970 to 1997 show that ~60% of its annual rainfall (710 mm) fall in the JAS season (414 mm) (Fig. 2a) when the monsoon rainfall is at its most northerly location. EC-Earth simulated rainfall shows a similar seasonal cycle (Fig. 2b) but has a dry bias of 47% over the Sahel and dry bias of 22% over the Coast of Guinea during the NH summer. This dry bias in EC-Earth appears to result from both of the WAM being weaker and not reaching as far north as in observations for the same period. For example, the CRU shows a WAM with a wet centre located over 8°–12° N, while the model simulation has a weaker maximum over around 7°–11° N. This dry bias in western Africa remains in the new model version EC-Earth3.3 with even higher resolution (Haarsma et al. 2020). The physical causes of this dry bias can be due to a wide range of deficiencies in the model parameterisations of land surface and cloud physics, which needs to be investigated in further detail.

The seasonal cycle structure in rainfall remains similar in 1901–2015 mean for CRU data (Fig. 2c) and the 850–1850 mean for EC-Earth 'last millennium' simulation (Fig. 2d). We notice that the WAM was stronger, and extended further northward, in the long-term mean in both data sources comparing their 1970–1997 mean. The weaker WAM in 1970–1997 mean both in observation and simulation reflects the well-known persistent drought period in West Africa from the early 1970s to the 1990s. The mean monsoon rainfall of the last millennium from EC-Earth simulation shows a more vigorous intensity in the JAS season than the 1901–2015 mean rainfall from CRU data. This is consistent with the results from previous studies, suggesting that West Africa and the Sahel region were wetter in several episodes during the 850–1850 period than during the twentieth century (Shanahan et al. 2009). In the following analysis, we focus on July–September (JAS) when West Africa receives most of its rainfall.

Fig. 2 Latitudinal-time distribution of terrestrial rainfall (unit: mm/month) over West Africa (5°–20° N, 20° W–30° E). **a** From CRU observational data averaged for 1970–1997; **b** from EC-Earth “historical” simulation averaged for 1970–1997; **c** from CRU monthly mean data averaged for 1901–2015; **d** from EC-Earth ‘last millennium’ simulation averaged for 850–1850

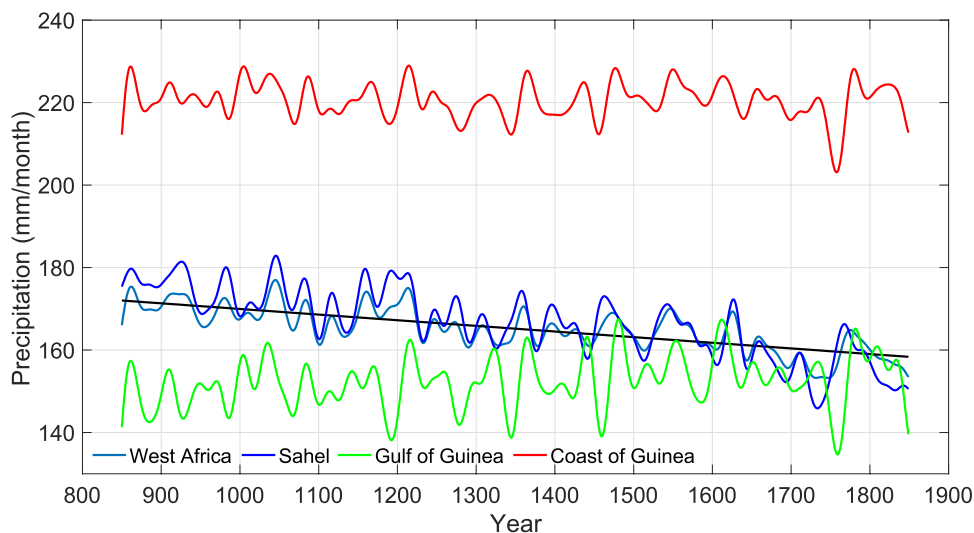


4.2 Long-term trend in rainfall

The multidecadal variability is apparent in the 850–1850 rainfall variation, with a significant decreasing trend in summer rainfall occurring over the West Africa domain (Fig. 3). The decreasing trend is associated to the decline of insolation in the Northern Hemisphere at the top of the atmosphere. The insolation at the top of the atmosphere is

determined by the solar irradiance (emitted energy from the Sun) and the Earth’s orbit (the latitudinal distribution of the short-wave solar energy). The trend in insolation is mostly due to changes in orbital forcing (Schmidt et al. 2011). During the last millennium, the slight changes in eccentricity and obliquity, and a 20-day shift in perihelion (from 15 December to 4 January), together with give a 7.8 W/m^2 decrease in insolation in August at 15°N . During

Fig. 3 The variation of summer rainfall (JAS mean, unit: mm/month) from 850 to 1850 over western Africa (light blue, linear trend shown in black), Sahel (blue), Coast of Guinea (red) and Gulf of Guinea (green). A Butterworth low-pass filter with 30-year cut-off frequency has been applied to the time series



the 1001-year simulated period from 850 to 1850 CE, WAM rainfall decreased by 7.5%. For the West African continent as a whole, the long-term linear trends comprise a wet period in the beginning and a dry period in the later part, mostly consistent with paleoclimate proxy data derived from lake sediments (Maley 1993; Shanahan et al. 2009; Street-Perrott et al. 2000). The variation of West African rainfall mainly reflects the rainfall variability in the Sahel. An apparent trend is seen in the rainfall in the Sahel region, which has decreased by about 12% during the last millennium. There is no noticeable trend over the Coast of Guinea. A slightly increasing rainfall trend over the Gulf of Guinea. A visible wet–dry multidecadal oscillation is apparent in all of the time series.

A spatial trend analysis of the total JAS rainfall over North Africa also reveals a drying trend over the 850–1850 period, centred over 10°–18° N, extending from east to west over the entire continent (Fig. 4a). The rainfall centre falls right into the Sahel domain as defined in Fig. 1a. Its southern neighbour Coast of Guinea exhibits both weak negative and positive rainfall trends, which explains the previous results in Fig. 3 where no trend is observed in its rainfall index time series. The positive rainfall trend is instead centred over the Gulf of Guinea and equatorial Atlantic. The rainfall trend pattern exhibits a latitudinal dipole, which is also seen in more recent observations (e.g. trend in 1998–2013) (Odoulami and Akinsanola 2018). This dipole pattern is typically established through a change of the surface temperature gradient that modulates the monsoon flow and the African Easterly Jet (Janicot et al. 1998; Losada et al. 2010). The spatial trend in surface air temperature shows a contrast pattern with cooling in Sahara, decreasing southward but covering most of northern Africa, and warming in the north part of the Sahel. During the 850–1850 CE period, the large-area cooling trend is consistent with the declining insolation in Northern Hemisphere summer due to changes in the

Earth's orbit. This cooling trend, which weakens the latitudinal temperature gradient, results in a weakening of the WAM and leads to drier conditions in the Sahel region as seen in Fig. 4a. The dry conditions at the surface reduce the evaporative cooling in the monsoon season and lead to anomalous warming effect, as shown from the surface latent heat flux (Fig. 4c). This warming effect prevails over the surface cooling, caused by insolation change, and eventually results in warming over 15–20°N.

4.3 Rainfall change between medieval climate anomaly and little ice age

In the EC-Earth “last millennium” simulation, as in other climate model simulations, the timing of the MCA and LIA slightly differs to those suggested by proxy-based reconstructions. The climate models are not expected to reproduce the exact climate evolution as the real world. It depends on the complexity of the physical processes built in the model system and the uncertainties in the climate forcing that is reconstructed from proxy data (Ljungqvist et al. 2019b). The WAM is driven and modulated by the thermal conditions over the African continent and adjacent ocean, therefore in the model system, the rainfall variability would be dynamically consistent with the temperature variability. According to the evolution of global mean temperature in EC-Earth simulation (Ljungqvist et al. 2019b), here we define the relatively warm period around 900–1200 CE as MCA and the cold period at the later part from 1550 to 1850 CE as LIA in the EC-Earth “last millennium” simulation. We show a climate change pattern between the two periods in Fig. 5. A similar latitudinal dipole pattern in the long-term trend in Fig. 4a is observed, with wet conditions in Sahel/Sahara and dry conditions over the Gulf of Guinea (including part of the coastline, as defined in Sect. 2). Ljungqvist et al. (2016) also identified dry conditions along the Coast of Guinea in their anomaly maps of the 11th to thirteenth centuries.

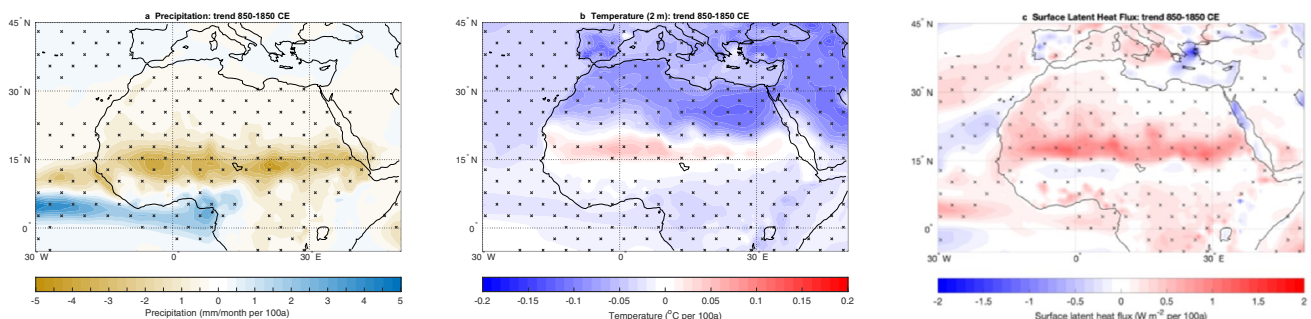


Fig. 4 The linear trend over the northern Africa region, **a** for JAS mean rainfall (unit: mm/month per 100 years); **b** for JAS mean 2-m air temperature (unit: °C per 100 years); **c** for JAS mean surface latent heat flux (unit: W/m² per 100 years, vertical flux defined as positive

downward). The trend is calculated for each model grid for the period 850–1850. Stippling indicates the trends that are significant at the 95% confidence level

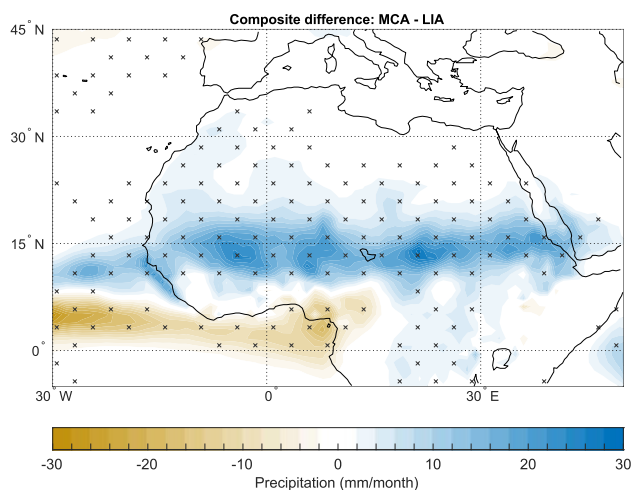


Fig. 5 The change in JAS rainfall (unit: mm/month) between medieval climate anomaly (MCA, averaged for 900–1200 CE) and little ice age (LIA, averaged for 1550–1850 CE). Stippling indicates the differences that are significant at the 95% confidence level

An overall wetter MCA and a drier LIA over the Sahel reflect the WAM's response to the long-term trend of orbital forcing and solar forcing. However, the internal impacts of the ocean–atmosphere system also play a role. For instance, previous work showed that the wetter conditions during the MCA are related to the dominant positive phase of the AMO (Kuhnert and Mulitza 2011; Mann et al. 2009; Wang et al. 2017). The connection is associated with a northward shift of the Atlantic ITCZ (Ting et al. 2011b) and typically increases moisture flux into the western Sahel from Atlantic sources in the south and west (Delworth et al. 2007; Martin et al. 2014; Zhang and Delworth 2006). Below we further examine the effect of ocean–atmosphere coupling on West African rainfall variability.

4.4 West African rainfall variability pattern and its relation to SST

Studies using observational data and atmospheric modeling have confirmed that SST anomalies over the equatorial Atlantic are responsible for the summer rainfall dipole pattern over West Africa at interannual timescales (Rodwell and Hoskins 1996; Rowell et al. 1995). However, the anticorrelation is non-stationary (Losada et al. 2012; Mohino et al. 2011). For low-frequency variability, observation data shows that the inter-hemispheric SST pattern is strongly related to the multidecadal variability in 100 years of instrumental data (1901–2002), in this coupling mode the rainfall exhibits same-signed anomalies over West Africa (Joly et al. 2007). Most ocean–atmosphere coupled climate models failed to capture the low-frequency SST-rainfall coupling evident in the observations (Joly et al. 2007; Martin et al. 2014). For

multidecadal climate variability, an only 100-year long dataset can hardly yield statistically significant results. Here we use the 1001-year model output to revisit the co-variability question between the SST and the West African rainfall. The SVD analysis is performed on JAS mean precipitation and SST, and all the data is detrended, and further filtered by removing high-frequency fluctuations less than 10 years.

As shown in Figs. 6 and 8, the first two leading SVD modes account for ~90% of the total square covariance. The first mode accounts for ~60% (Fig. 6) and the second accounts for ~30% (Fig. 8). The patterns represent robust modes of variability and are consistent with the results of a rotated EOF performed on JAS rainfall over West Africa (not shown). SVD mode 1 indicates an Atlantic Niño type SST variability pattern, with a strong warm SST centre over the equatorial Atlantic Ocean (Fig. 6a), which affects the Gulf of Guinea's rainfall variability and its surrounding coast (Fig. 6b). The Atlantic Niño is a zonal mode of tropical Atlantic variability (Zebiak 1993). It represents changes in the cold tongue at the eastern part of the basin, just south of the Equator. The Atlantic Niño is known to affect interannual climate variability over adjacent and remote regions. A warming SST could lead to increases of rainfall over the Gulf of Guinea coast (Losada et al. 2010; Mohino et al. 2011), and this covariant feature has been shown in SVD1 patterns. During 850–1850, the statistically significant period of variability appears at decadal and multidecadal timescales, i.e., 10–14 years and 20–40 years, in both SST and rainfall field (Fig. 6c, d). A 60–80 years co-variability also shows up but only statistically significant in SST field. The regression maps in Fig. 7 demonstrate the physical processes of how the SST anomalies over equatorial Atlantic affect the rainfall over the Gulf of Guinea. The warming SSTs (Fig. 6a) over the eastern tropical Atlantic increases the amount of moisture in the atmosphere (Fig. 7a) and forms an anomalous low pressure over this area (Fig. 7b). The low pressure weakens the meridional pressure gradient between the Saharan Heat Low and the equatorial Atlantic and leads to anomalous northeasterly (Fig. 7c). This decreases the southwesterly moisture flux into the Sahel and confines the moisture flux convergence at the equatorial region (Fig. 7d), resulting in reduced rainfall over the Sahel and increased rainfall in Gulf of Guinea and its surrounding coastal area. Meanwhile, there is an increased zonal pressure gradient (Fig. 7b), which enhances the westerlies (Fig. 7c) and brings more moisture to the Coast of Guinea (Fig. 7d).

The homogeneous correlation maps of the second SVD mode depict a monopole rainfall variability pattern extending from the Coast of Guinea to the Sahara region (Fig. 8b), connected to an AMO-like pattern of SST anomalies located in the North Atlantic and the Mediterranean (Fig. 8a) and consistent with findings based on shorter data for the past few decades (Park et al. 2016; Sheen et al. 2017). They also

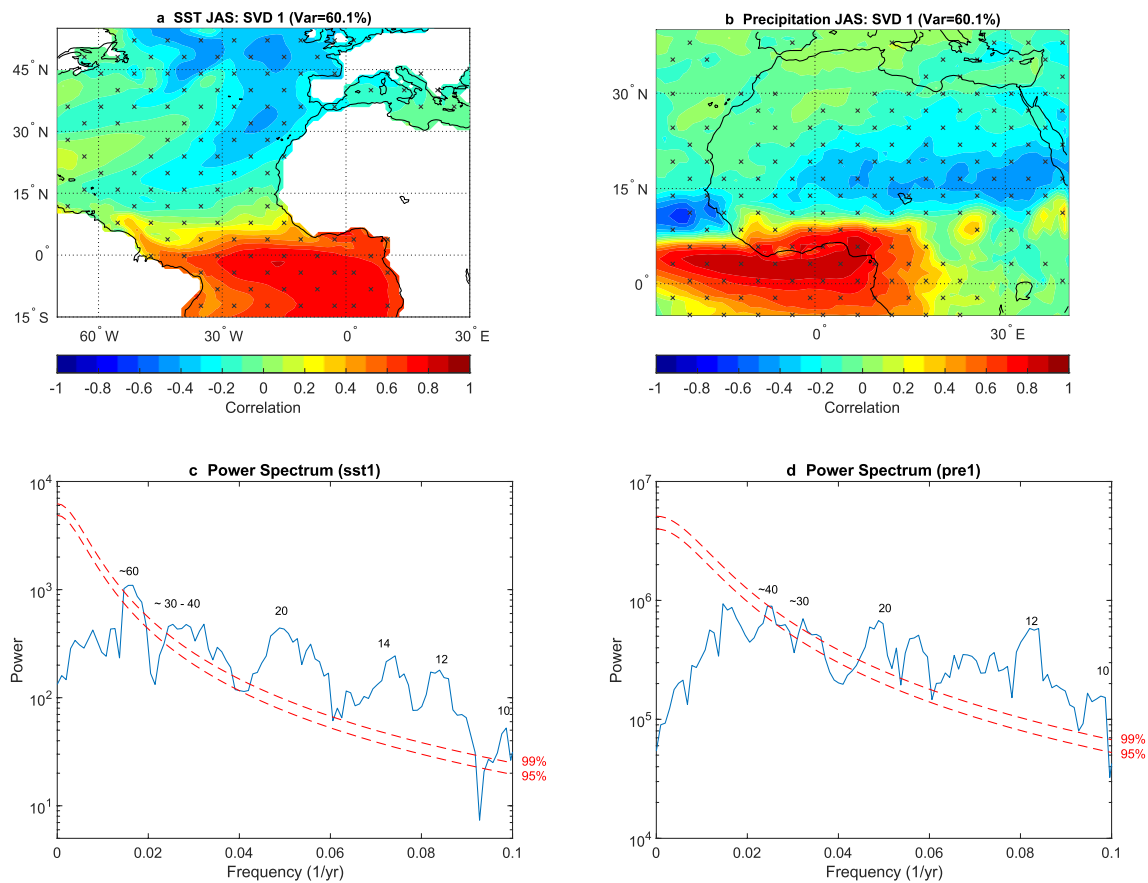


Fig. 6 The first leading SVD mode (explained 60.1% of variance) presented as homogeneous correlation maps for **a** SST mode 1 and **b** rainfall mode 1. Stippling indicates correlations that are significant at the 95% confidence level, and the maps boundaries indicate the areas

co-vary at decadal to multi-decadal timescale, i.e. a ~ 10 – 14 and ~ 20 – 30 years oscillation period (Fig. 8c, d). The maximum variability in the SST field is centred at the latitudes of maximum Atlantic meridional overturning circulation (AMOC) around 40° – 50° N. This SST pattern affects the rainfall variability over a large area of North Africa including Sahara, with the maximum variability occurring over the Sahel, expanding to its far eastern part. The rainfall variability is centred at 15° N, poleward of the mean JAS rainfall maximum (10° – 12° N) (Fig. 2d), and maximum humidity anomalies are located in the north-eastern part of Sahel and Sahara (Fig. 9a). The warm SSTs in the North Atlantic and the Mediterranean corresponds to a deepening of the thermally induced low-pressure area across the Sahara (Saharan Heat Low) (Fig. 9b), leading to a stronger meridional pressure gradient and strengthened cyclonic circulation (Fig. 9c). More moisture is transported into the Sahel from the Atlantic by enhanced west/southwesterly, leading to a moisture flux convergence over the region and a northward shift of the rainfall. There is also a slight increase of moisture being transported from the Mediterranean by enhanced

used when performing the SVD. The power spectrum for the expansion coefficients of **c** SST mode 1 and **d** rainfall mode 1, the numbers labelled are timescales of variability in years

northerlies (Fig. 9d), leading to increased rainfall across northern Africa.

5 Discussion and conclusion

The ‘last millennium’ EC-Earth climate model simulation has shown a latitudinal rainfall dipole over West African rainfall at decadal to multidecadal timescales. The North Atlantic SST variability modulates the rainfall dipole. The rainfall dipole also appears in the long-term trend, and centennial variability between the MCA and LIA, indicating that the external forcing can amplify the dipole pattern through thermal forcing and feedback.

From the SVD analysis, we notice that the dipole-like rainfall pattern appears in SVD1 but not in SVD2. We conclude that the tropical SST anomalies are the primary driver for the dipole-like pattern, predominantly on decadal to multidecadal timescales (~ 10 – 30 years). The second SVD presents a monopole rainfall pattern extending from the Coast of Guinea to the Sahara, centred on the Sahel

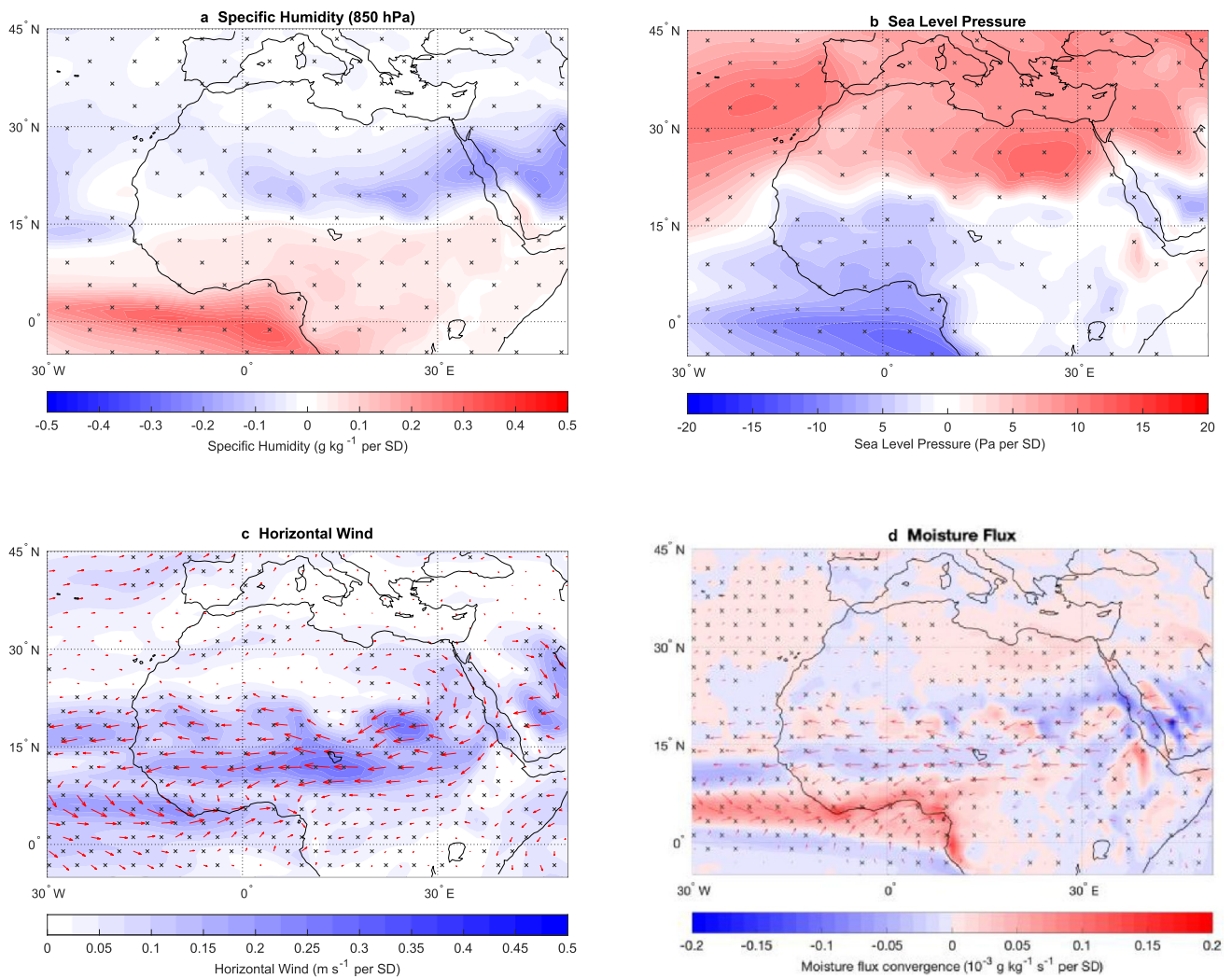


Fig. 7 Regression maps against the SVD1 SST expansion coefficient for **a** specific humidity at 850 hPa, **b** sea level pressure, **c** horizontal wind (vector) and wind speed (shading) at 850 hPa, and **d** moisture flux (vector) and its convergence (shading) at 850 hPa, expressed in

units per standard deviation (SD) change in the expansion coefficient. Stippling indicates regressions that are significant at the 95% confidence level

region. This monopole rainfall pattern in West Africa varies at ~ 10 – 30 years' timescale, modulated by the North Atlantic and Mediterranean SST anomalies. It confirmed the previous study showing that AMO plays a significant role in forcing the 20th-century multidecadal variations in Sahel summer rainfall (Zhang and Delworth 2006). In their model simulation, the positive AMO phase leads to a northward shift of the ITCZ. It is associated with anomalous southwesterly surface winds over the Sahel, leading to a surface moisture convergence and enhancing the Sahel's rainfall. We confirm that this process is statistically robust in our "last millennium" model simulation data. It also supports the theory that the negative AMO phase from the 1970s to 1990s largely contributed to the persistent droughts in the Sahel during this period. A proper simulation of the remote SST influences on the west African rainfall appears to be

a key for predictive skill at multidecadal timescales (Martin et al. 2014). The predict skill in west African rainfall is likely associated with significant AMO prediction skill (García-Serrano et al. 2015; Guemas et al. 2015; Mohino et al. 2016). Notably, changes in the Sahelian rainfall are not significant in some PMIP3 last millennium simulations (Stevenson et al. 2018). The reason might depend on how well the internal variability is represented in different "last millennium" simulations.

The contribution of Mediterranean SST forcing on Sahel rainfall shown in the second SVD is similar to those identified by Park et al. (2016) with respect to SST forcing from different ocean basins. While the increased specific humidity across the Sahel mainly reflects increased moisture flux from the Atlantic, the warm SSTs in the North Atlantic and the Mediterranean drive the deepening of the thermally induced

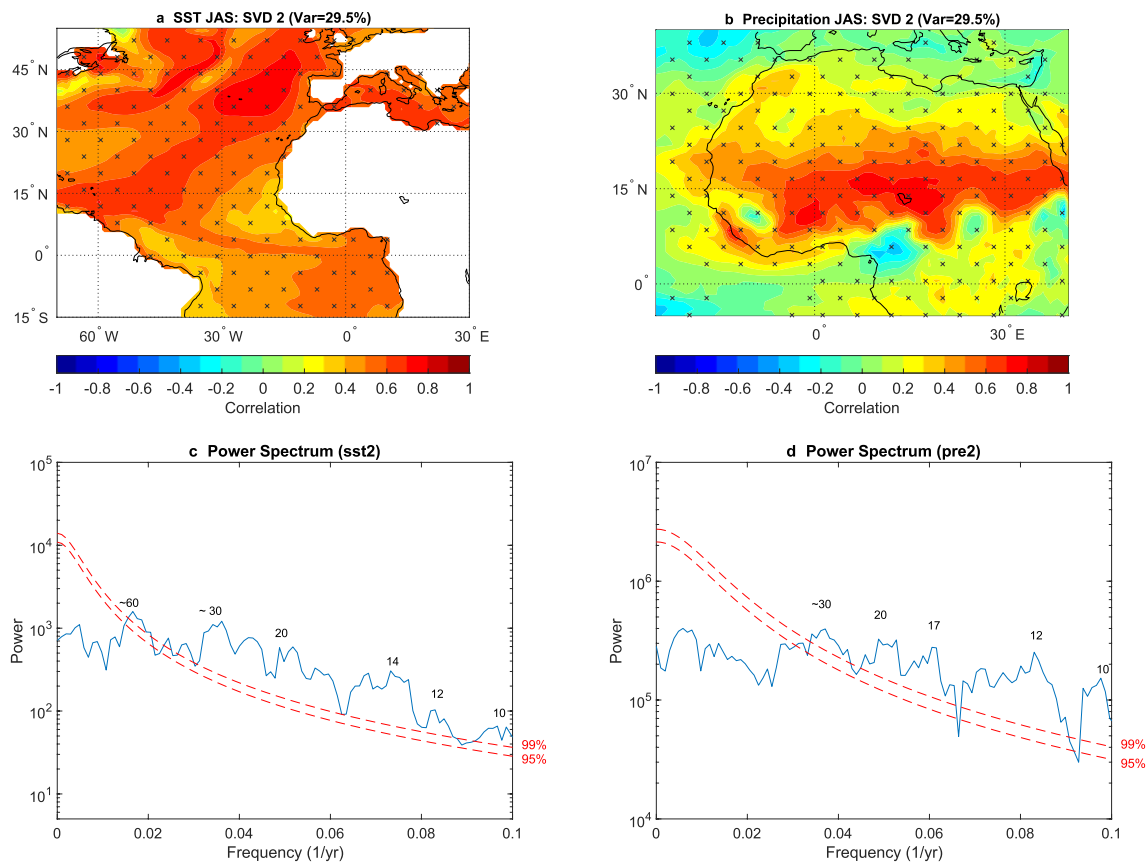


Fig. 8 The second leading SVD mode (explained 29.5% of variance) presented as homogeneous correlation maps for **a** SST mode 2 and **b** rainfall mode 2. The power spectrum for the expansion coefficients of

c SST mode 2 and **d** rainfall mode 2, the numbers labelled are time-scales of variability in years. Stippling in **a** and **b** indicates correlations that are significant at the 95% confidence level

low-pressure area across Sahara. Moisture transported into Sahara with the anomalous northeasterly winds can also have helped strengthen the low-pressure area by enhancing the convective cells by releasing latent heat. In our fully coupled “last millennium” simulation, the SST forcing in North Atlantic and the Mediterranean and accompanied low-pressure system dominates the Sahel’s rainfall.

Several modelling studies have suggested that the anthropogenic aerosol forcing and GHG forcing are the most critical drivers for the drying trend in the Sahel in late twentieth century (Biasutti and Giannini 2006; Booth et al. 2012; Chang et al. 2011; Dong and Sutton 2015; Held et al. 2005; Hwang et al. 2013; Rotstayn and Lohmann 2002). The impacts of land cover changes to Sahel drought have been demonstrated by regional climate modelling (Boone et al. 2016; Wang et al. 2016).

The climate forcing for the last millennium include orbital forcing and solar irradiance, GHG, volcanic, and land-use changes (Schmidt et al. 2011, 2012). The GHG forcing and land-use changes are very small and do not yet reflect the anthropogenic forcing we have experienced during the twentieth century. The volcanic eruption is suggested to have initiated the LIA (Miller et al. 2012) and might have contributed to the centennial variability rainfall pattern between the MCA and LIA. Based on our model experiments, we find it plausible that the linear drying trend during the last millennium is the direct response to the orbital forcing, driven by the cooling trend in surface air temperature over the Sahara region. Both solar forcing, GHG forcing, and volcanic forcing and other minor forcing, can also affect the surface energy balance and amplify the rainfall response through atmospheric feedback (Rowell 2003) and land surface feedback (Nicholson 2013).

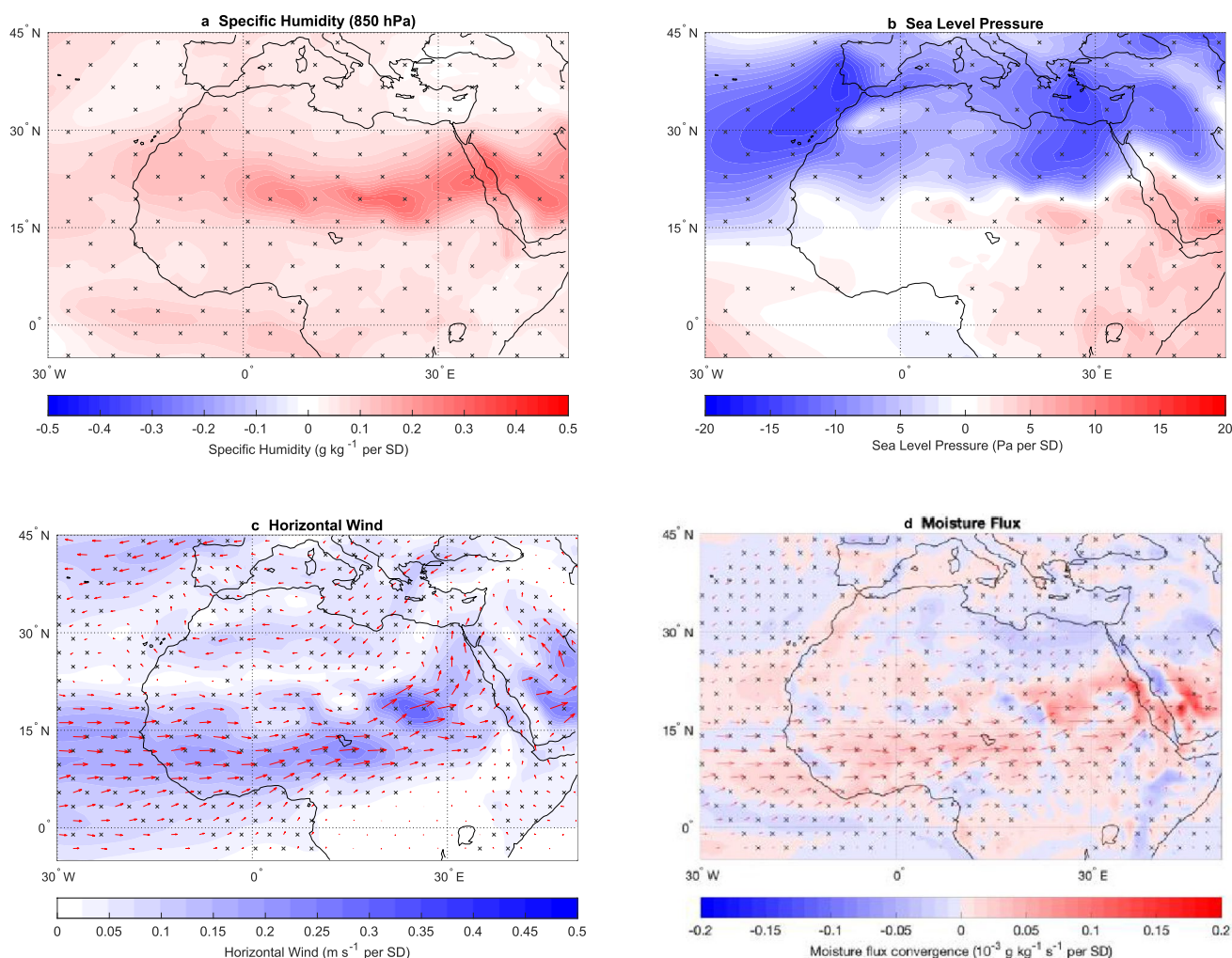


Fig. 9 Regressions against the SVD2 SST expansion coefficient for **a** specific humidity at 850 hPa, **b** sea level pressure, **c** horizontal wind (vector) and wind speed (shading) at 850 hPa, and **d** moisture flux

(vector) and its convergence (shading) at 850 hPa, expressed in units per standard deviation change in the expansion coefficient. Stippling indicates regressions that are significant at the 95% confidence level

Acknowledgements This work was supported by the Swedish Research Council (Vetenskapsrådet, Grant nos. 2013-06476 and 2017-04232). F.C.L. was supported by the Swedish Research Council (Vetenskapsrådet, Grant no 2018-01272), and worked with this article as a Pro Futura Scientia XIII Fellow funded by the Swedish Collegium for Advanced Study through Riksbankens Jubileumsfond. The ‘last millennium’ EC-Earth simulation is performed on ECMWF’s computing and archive facilities. The ‘historical’ EC-Earth simulation and all model data analyses were performed by resources provided by the Swedish National Infrastructure for Computing (SNIC) at the National Supercomputer Centre (NSC) partially funded by the Swedish Research Council through Grant agreement no. 2016-07213.

Author contributions QZ conceived the research idea and designed the work. EB analysed the data and prepared the figures. QZ wrote the manuscript, EB and FCL commented, edited and provided input to the manuscript. QL performed the EC-Earth simulations.

Funding Open access funding provided by Stockholm University.

Open Access This article is licensed under a Creative Commons Attribution 4.0 International License, which permits use, sharing, adaptation, distribution and reproduction in any medium or format, as long as you give appropriate credit to the original author(s) and the source, provide a link to the Creative Commons licence, and indicate if changes were made. The images or other third party material in this article are included in the article’s Creative Commons licence, unless indicated otherwise in a credit line to the material. If material is not included in the article’s Creative Commons licence and your intended use is not permitted by statutory regulation or exceeds the permitted use, you will need to obtain permission directly from the copyright holder. To view a copy of this licence, visit <http://creativecommons.org/licenses/by/4.0/>.

References

- Berger AL (1978) Long-term variations of caloric insolation resulting from the earth's orbital elements. *Quat Res* 9:139–167
- Berntell E, Zhang Q, Chafik L, Körnich H (2018) Representation of multidecadal Sahel rainfall variability in 20th century reanalyses. *Sci Rep* 8:10937
- Biasutti M (2013) Forced Sahel rainfall trends in the CMIP5 archive. *J Geophys Res Atmos* 118:1613–1623
- Biasutti M, Giannini A (2006) Robust Sahel drying in response to late 20th century forcings. *Geophys Res Lett*. <https://doi.org/10.1029/2006gl026067>
- Boone AA et al (2016) The regional impact of land-use land-cover change (LULCC) over West Africa from an ensemble of global climate models under the auspices of the WAMME2 project. *Clim Dyn* 47:3547–3573. <https://doi.org/10.1007/s00382-016-3252-y>
- Booth BB, Dunstone NJ, Halloran PR, Andrews T, Bellouin N (2012) Aerosols implicated as a prime driver of twentieth-century North Atlantic climate variability. *Nature* 484:228–232
- Bouillon S, Maqueda MAM, Legat V, Fichet T (2009) An elastic–viscous–plastic sea ice model formulated on Arakawa B and C grids. *Ocean Model* 27:174–184
- Bretherton CS, Smith C, Wallace JM (1992) An intercomparison of methods for finding coupled patterns in climate data. *J Clim* 5:541–560
- Caminade C, Terray L (2010) Twentieth century Sahel rainfall variability as simulated by the ARPEGE AGCM, and future changes. *Clim Dyn* 35:75–94
- Chang C-Y, Chiang JCH, Wehner MF, Friedman AR, Ruedy R (2011) Sulfate aerosol control of tropical Atlantic climate over the twentieth century. *J Clim* 24:2540–2555. <https://doi.org/10.1175/2010jcli4065.1>
- Crowley TJ, Unterman MB (2013) Technical details concerning development of a 1200 yr proxy index for global volcanism. *Earth Syst Sci Data* 5:187–197
- Dai A, Lamb PJ, Trenberth KE, Hulme M, Jones PD, Xie P (2004) The recent Sahel drought is real. *Int J Climatol J R Meteorol Soc* 24:1323–1331
- Delworth TL, Zhang R, Mann ME (2007) Decadal to centennial variability of the Atlantic from observations and models. *Ocean Circ Mech Impacts Past Future Changes Merid Overturning* 131–148
- Dong B, Sutton R (2015) Dominant role of greenhouse-gas forcing in the recovery of Sahel rainfall. *Nat Clim Change* 5:757–760. <https://doi.org/10.1038/nclimate2664>
- Emery W, Thomson R (2001) Time-series analysis methods. *Data Anal Methods Phys Oceanogr* 371:371–567
- Folland C, Palmer T, Parker D (1986) Sahel rainfall and worldwide sea temperatures, 1901–85. *Nature* 320:602–607
- García-Serrano J, Guemas V, Doblas-Reyes F (2015) Added-value from initialization in predictions of Atlantic multi-decadal variability. *Clim Dyn* 44:2539–2555
- Giannini A, Saravanan R, Chang P (2003) Oceanic forcing of Sahel rainfall on interannual to interdecadal time scales. *Science* 302:1027–1030
- Guemas V, García-Serrano J, Mariotti A, Doblas-Reyes F, Caron LP (2015) Prospects for decadal climate prediction in the Mediterranean region. *Q J R Meteorol Soc* 141:580–597
- Haarsma R et al (2020) HighResMIP versions of EC-Earth: EC-Earth3P and EC-Earth3P-HR—description, model computational performance and basic validation. *Geosci Model Dev* 13:3507–3527. <https://doi.org/10.5194/gmd-13-3507-2020>
- Hansen J, Sato M (2004) Greenhouse gas growth rates. *Proc Natl Acad Sci USA* 101:16109–16114
- Harris I, Jones PD, Osborn TJ, Lister DH (2014) Updated high-resolution grids of monthly climatic observations—the CRU TS3. 10 Dataset *Int J Climatol* 34:623–642
- Hazeleger W et al (2012) EC-Earth V2.2: description and validation of a new seamless earth system prediction model. *Clim Dyn* 39:2611–2629
- Held IM, Delworth TL, Lu J, Findell KL, Knutson TR (2005) Simulation of Sahel drought in the 20th and 21st centuries. *Proc Natl Acad Sci USA* 102:17891. <https://doi.org/10.1073/pnas.0509057102>
- Hoerling M, Hurrell J, Eischeid J, Phillips A (2006) Detection and attribution of twentieth-century northern and southern African rainfall change. *J Clim* 19:3989–4008. <https://doi.org/10.1175/jcli3842.1>
- Hwang Y-T, Frierson DMW, Kang SM (2013) Anthropogenic sulfate aerosol and the southward shift of tropical precipitation in the late 20th century. *Geophys Res Lett* 40:2845–2850. <https://doi.org/10.1002/grl.50502>
- Janicot S (1992) Spatiotemporal variability of West African rainfall. Part I: regionalizations and typings. *J Clim* 5:489–497
- Janicot S, Sultan B (2001) Intra-seasonal modulation of convection in the West African monsoon. *Geophys Res Lett* 28:523–526
- Janicot S, Harzallah A, Fontaine B, Moron V (1998) West African monsoon dynamics and eastern equatorial Atlantic and Pacific SST anomalies (1970–88). *J Clim* 11:1874–1882
- Janowiak JE (1988) An investigation of interannual rainfall variability in Africa. *J Clim* 1:240–255
- Joly M, Voltaire A (2010) Role of the Gulf of Guinea in the interannual variability of the West African monsoon: what do we learn from CMIP3 coupled simulations? *Int J Climatol* 30:1843–1856
- Joly M, Voltaire A, Douville H, Terray P, Royer J-F (2007) African monsoon teleconnections with tropical SSTs: validation and evolution in a set of IPCC4 simulations. *Clim Dyn* 29:1–20
- Kageyama M et al (2018) The PMIP4 contribution to CMIP6—part 1: overview and over-arching analysis plan. *Geosci Model Dev* 11:1033–1057
- Kandji ST et al (2006) Opportunities for linking climate change adaptation and mitigation through agroforestry systems. *World Agroforestry into the Future World Agroforestry Centre, Nairobi*, pp 113–122
- Knight JR, Folland CK, Scaife AA (2006) Climate impacts of the Atlantic multidecadal oscillation. *Geophys Res Lett*. <https://doi.org/10.1029/2006GL026242>
- Kuhnert H, Mulitza S (2011) Multidecadal variability and late medieval cooling of near-coastal sea surface temperatures in the eastern tropical North Atlantic. *Paleoceanography* 26:PA4224. <https://doi.org/10.1029/2011PA002130>
- Lavender SL et al (2018) Estimation of the maximum annual number of North Atlantic tropical cyclones using climate models. *Sci Adv* 4:eaat6509. <https://doi.org/10.1126/sciadv.aat6509>
- Liu Z, Zhang Q, Wu L (2004) Remote impact on tropical Atlantic climate variability: statistical assessment and dynamic assessment. *J Clim* 17:1529–1549
- Ljungqvist FC, Krusic PJ, Sundqvist HS, Zorita E, Brattström G, Frank D (2016) Northern Hemisphere hydroclimate variability over the past twelve centuries. *Nature* 532:94–98
- Ljungqvist FC et al (2019) Centennial-scale temperature change in last millennium simulations and proxy-based reconstructions. *J Clim* 32:2441–2482
- Ljungqvist FC et al (2019) European warm-season temperature and hydroclimate since 850 CE. *Environ Res Lett* 14:084015. <https://doi.org/10.1088/1748-9326/ab2c7e>
- Losada T, Rodríguez-Fonseca B, Janicot S, Gervois S, Chauvin F, Ruti P (2010) A multi-model approach to the Atlantic equatorial mode: impact on the West African monsoon. *Clim Dyn* 35:29–43

- Losada T, Rodriguez-Fonseca B, Mohino E, Bader J, Janicot S, Mechoso C (2012) Tropical SST and Sahel rainfall: a non-stationary relationship. *Geophys Res Lett* 39:L12705. <https://doi.org/10.1029/2012GL052423>
- Macfarling Meure C et al (2006) Law Dome CO₂, CH₄ and N₂O ice core records extended to 2000 years BP. *Geophys Res Lett* 33:L14810. <https://doi.org/10.1029/2006GL026152>
- Madec G (2008) NEMO ocean general circulation model reference manuel. In: Internal report. LODYC/IPSL Paris
- Maley J (1993) Chronologie calendaire des principales fluctuations du lac Tchad au cours du dernier millénaire Datation et Chronologie dans le Bassin du Lac Tchad ORSTOM, Paris, pp 161–163
- Mann ME, Lees JM (1996) Robust estimation of background noise and signal detection in climatic time series. *Clim Change* 33:409–445
- Mann ME et al (2009) Global signatures and dynamical origins of the Little Ice Age and Medieval Climate Anomaly. *Science* 326:1256–1260
- Martin ER, Thorncroft C, Booth BB (2014) The multidecadal Atlantic SST—Sahel rainfall teleconnection in CMIP5 simulations. *J Clim* 27:784–806
- Masih I, Maskey S, Mussá F, Trambauer P (2014) A review of droughts on the African continent: a geospatial and long-term perspective. *Hydrol Earth Syst Sci* 18:3635–3649
- Miller GH et al (2012) Abrupt onset of the Little Ice Age triggered by volcanism and sustained by sea–ice/ocean feedbacks. *Geophys Res Lett*. 39:L02708. <https://doi.org/10.1029/2011GL050168>
- Mohino E et al (2011) Changes in the interannual SST-forced signals on West African rainfall. AGCM intercomparison. *Clim Dyn* 37:1707–1725
- Mohino E, Keenlyside N, Pohlmann H (2016) Decadal prediction of Sahel rainfall: where does the skill (or lack thereof) come from? *Clim Dyn* 47:3593–3612
- Mulitza S et al (2010) Increase in African dust flux at the onset of commercial agriculture in the Sahel region. *Nature* 466:226
- Nash DJ et al (2016) African hydroclimatic variability during the last 2000 years. *Quat Sci Rev* 154:1–22
- Nicholson SE (1980) The nature of rainfall fluctuations in subtropical West Africa. *Mon Weather Rev* 108:473–487
- Nicholson SE (2013) The West African Sahel: a review of recent studies on the rainfall regime and its interannual variability. *ISRN Meteorol* 2013:453521
- Nicholson SE, Palao IM (1993) A re-evaluation of rainfall variability in the Sahel. Part I. Characteristics of rainfall fluctuations. *Int J Climatol* 13:371–389
- Nnamchi HC, Li J (2011) Influence of the South Atlantic Ocean dipole on West African summer precipitation. *J Clim* 24:1184–1197
- Nouaceur Z, Murărescu O (2016) Rainfall variability and trend analysis of annual rainfall in North Africa. *Int J Atmos Sci* 2016:7230450
- Odoulami RC, Akinsanola A (2018) Recent assessment of West African summer monsoon daily rainfall trends. *Weather* 73:283–287
- Otero N, Mohino E, Gaetani M (2016) Decadal prediction of Sahel rainfall using dynamics-based indices. *Clim Dyn* 47:3415–3431
- Palmer T (1986) Influence of the Atlantic, Pacific and Indian oceans on Sahel rainfall. *Nature* 322:251–253
- Park J-Y, Bader J, Matei D (2016) Anthropogenic Mediterranean warming essential driver for present and future Sahel rainfall. *Nat Clim Change* 6:941–945
- Pongratz J, Reick C, Raddatz T, Claussen M (2008) A reconstruction of global agricultural areas and land cover for the last millennium. *Glob Biogeochem Cycles* 22:GB3018. <https://doi.org/10.1029/2007GB003153>
- Rodríguez-Fonseca B et al (2011) Interannual and decadal SST-forced responses of the West African monsoon. *Atmos Sci Lett* 12:67–74
- Rodríguez-Fonseca B et al (2015) Variability and predictability of West African droughts: a review on the role of sea surface temperature anomalies. *J Clim* 28:4034–4060
- Rodwell MJ, Hoskins BJ (1996) Monsoons and the dynamics of deserts. *Q J R Meteorol Soc* 122:1385–1404
- Roehrig R, Bouniol D, Guichard F, Hourdin F, Redelsperger J-L (2013) The present and future of the West African monsoon: a process-oriented assessment of CMIP5 simulations along the AMMA transect. *J Clim* 26:6471–6505
- Rotstayn LD, Lohmann U (2002) Tropical rainfall trends and the indirect aerosol effect. *J Clim* 15:2103–2116
- Rowell DP (2003) The impact of Mediterranean SSTs on the Sahelian rainfall season. *J Clim* 16:849–862
- Rowell DP, Folland CK, Maskell K, Ward MN (1995) Variability of summer rainfall over tropical North Africa (1906–92): observations and modelling. *Q J R Meteorol Soc* 121:669–704
- Schmidt G et al (2011) Climate forcing reconstructions for use in PMIP simulations of the last millennium (v1.0). *Geosci Model Dev* 4:33–45
- Schmidt G et al (2012) Climate forcing reconstructions for use in PMIP simulations of the Last Millennium (v1.1). *Geosci Model Dev* 5:185–191
- Shanahan TM et al (2009) Atlantic forcing of persistent drought in West Africa. *Science* 324:377–380
- Sheen K, Smith D, Dunstone N, Eade R, Rowell D, Vellinga M (2017) Skilful prediction of Sahel summer rainfall on inter-annual and multi-year timescales. *Nat Commun* 8:1–12
- Stevenson S et al (2018) Climate variability, volcanic forcing, and last millennium hydroclimate extremes. *J Clim* 31:4309–4327
- Stocker T et al (2013) IPCC, 2013: Climate change 2013: the physical science basis. Contribution of working group I to the Fifth Assessment report of the Intergovernmental Panel on Climate Change. Cambridge University Press, Cambridge
- Street-Perrott FA et al (2000) Drought and dust deposition in the West African Sahel: a 5500-year record from Kajamarum Oasis, north-eastern Nigeria. *Holocene* 10:293–302
- Sultan B, Janicot S (2003) The West African monsoon dynamics. Part II: The “preonset” and “onset” of the summer monsoon. *J Clim* 16:3407–3427
- Talbot M, Delibrias G (1977) Holocene variations in the level of Lake Bosumtwi, Ghana. *Nature* 268:722
- Taylor KE, Stouffer RJ, Meehl GA (2012) An overview of CMIP5 and the experiment design. *Bull Am Meteorol Soc* 93:485–498
- Ting M, Kushnir Y, Seager R, Li C (2011a) Robust features of Atlantic multi-decadal variability and its climate impacts. *Geophys Res Lett*. 38:L17705. <https://doi.org/10.1029/2011GL048712>
- Ting M, Kushnir Y, Seager R, Li C (2011b) Robust features of Atlantic multi-decadal variability and its climate impacts *Geophys Res Lett* 38
- Vieira LEA, Solanki SK (2010) Evolution of the solar magnetic flux on time scales of years to millennia. *Astron Astrophys* 509:A100
- Villamayor J, Mohino E (2015) Robust Sahel drought due to the inter-decadal Pacific oscillation in CMIP5 simulations. *Geophys Res Lett* 42:1214–1222
- Wang Y-M, Lean J, Sheeley N Jr (2005) Modeling the Sun’s magnetic field and irradiance since 1713. *Astrophys J* 625:522
- Wang G, Yu M, Xue Y (2016) Modeling the potential contribution of land cover changes to the late twentieth century Sahel drought using a regional climate model: impact of lateral boundary conditions. *Clim Dyn* 47:3457–3477
- Wang J, Yang B, Ljungqvist FC, Luterbacher J, Osborn TJ, Briffa KR, Zorita E (2017) Internal and external forcing of multidecadal Atlantic climate variability over the past 1,200 years. *Nat Geosci* 10:512–517
- Ward MN (1998) Diagnosis and short-lead time prediction of summer rainfall in tropical North Africa at interannual and multidecadal timescales. *J Clim* 11:3167–3191

- Wilks DS (2011) *Statistical methods in the atmospheric sciences*, vol 100. Academic Press, New York
- Xue Y et al (2016) West African monsoon decadal variability and surface-related forcings: second West African Monsoon Modeling and Evaluation Project Experiment (WAMME II). *Clim Dyn* 47:3517–3545
- Zebiak SE (1993) Air–sea interaction in the equatorial Atlantic region. *J Clim* 6:1567–1586
- Zhang R, Delworth TL (2006) Impact of Atlantic multidecadal oscillations on India/Sahel rainfall and Atlantic hurricanes. *Geophys Res Lett* 33:L17712. <https://doi.org/10.1029/2006GL026267>

Publisher's Note Springer Nature remains neutral with regard to jurisdictional claims in published maps and institutional affiliations.